

**Investigation of the 2006 Drought and 2007 Flood Extremes at the Southern Great  
Plains Through an Integrative Analysis of Observations**

Xiquan Dong<sup>1</sup>, Baike Xi<sup>1</sup>, Aaron Kennedy<sup>1</sup>, Zhe Feng<sup>1</sup>, Jared K. Entin<sup>2</sup>, Paul R. Houser<sup>3</sup>, Robert  
A. Schiffer<sup>4</sup>, Tristan L'Ecuyer<sup>5</sup>, William S. Olson<sup>4</sup>, Kuo-lin Hsu<sup>6</sup>, W. Timothy Liu<sup>7</sup>, Bing Lin<sup>8</sup>,  
Yi Deng<sup>9</sup>, and Tianyu Jiang<sup>9</sup>

1. University of North Dakota

2. NASA HQ

3. George Mason University

4. University of Maryland at Baltimore County

5. Colorado State University

6. University California at Irvine

7. Jet Propulsion Lab.

8. NASA Langley Research Center

9. Georgia Institute of Technology

Re-Submitted to JGR-Atmosphere, July 14, 2010

Short title: SGP drought and flood

Point of contact: Xiquan Dong, University of North Dakota, 701-777-6991, [dong@aero.und.edu](mailto:dong@aero.und.edu)

**Abstract:** Hydrological years 2006 (HY06, 10/2005-09/2006) and 2007 (HY07, 10/2006-09/2007) provide a unique opportunity to examine hydrological extremes in the central US because there are no other examples of two such highly contrasting precipitation extremes occurring in consecutive years at the Southern Great Plains (SGP) in recorded history. The HY06 annual precipitation in the state of Oklahoma, as observed by the Oklahoma Mesonet, is around 61% of the normal (92.84 cm, based on the 1921-2008 climatology), which results in HY06 the second-driest year in the record. In particular, the total precipitation during the winter of 2005-06 is only 27% of the normal, and this winter ranks as the driest season. On the other hand, the HY07 annual precipitation amount is 121% of the normal and HY07 ranks as the seventh-wettest year for the entire state and the wettest year for the central region of the state. Summer 2007 is the second-wettest season for the state. Large-scale dynamics play a key role in these extreme events. During the extreme dry period (10/2005-02/2006), a dipole pattern in the 500-hPa GH anomaly existed where an anomalous high was over the southwestern U.S. region and an anomalous low was over the Great Lakes. This pattern is associated with inhibited moisture transport from the Gulf of Mexico and strong sinking motion over the SGP, both contributing to the extreme dryness. The precipitation deficit over the SGP during the extreme dry period is clearly linked to significantly suppressed cyclonic activity over the southwestern U.S., which shows robust relationship with the Western Pacific (WP) teleconnection pattern. The precipitation events during the extreme wet period (May-July 2007) were initially generated by active synoptic weather patterns, linked with moisture transport from the Gulf of Mexico by the northward low level jet, and enhanced by the mesoscale convective systems. Although the drought and pluvial conditions are dominated by large-scale dynamic patterns, we have demonstrated that the two positive feedback processes during the extreme dry and wet periods

found in this study play a key role to maintain and reinforce the length and severity of existing drought and flood events. For example, during the extreme dry period, with less clouds, LWP, PWV, precipitation, and thinner Cu cloud thickness, more net radiation was absorbed and used to evaporate water from the ground. The evaporated moisture, however, was removed by low-level divergence. Thus, with less precipitation and removed atmospheric moisture, more absorbed incoming solar radiation was used to increase surface temperature and to make the ground drier.

## 1. Introduction

Drought is the number one weather-related cause of death worldwide and ranks second in the weather-related causes of property damage within the United States during the past three decades [Raubert *et al.*, 2008; UCAR 2009]. Drought is defined as "a persistent and abnormal moisture deficiency having adverse impacts on vegetation, animals, or people" by the National Drought Policy Commission and is one of the most complicated but least understood natural hazards. Although quite a few researchers [e.g., Namias, 1978; Trenberth and Branstator, 1992; Trenberth and Guillemot, 1996; Schubert *et al.*, 2004a&b; Seager *et al.*, 2005] have investigated the fundamental causes of persistent droughts and linked the U.S. droughts with strong La Niña conditions in the tropical Pacific, our understanding of drought mechanisms is still limited. These include the physical "triggers" of a drought, dynamics in maintaining drought, and the processes that terminate a drought. Therefore, it remains a challenge for us to predict the onset and demise of a drought.

In contrast to persistent drought, flooding is a natural hazard characterized by heavy precipitation during short-time periods. Flooding ranks first among the weather-related causes of property damage in the United States and it is also the second largest weather-related cause of death worldwide. [Raubert *et al.*, 2008; UCAR 2009]. During recent years, floods, in particular, flash floods (heavy rain in a few hours), have caused billions of dollars in property damage within the United States. While floods are better understood compared to droughts, there are still challenges in their predictability because many factors contribute to the occurrences of floods. Flash floods are often triggered by frontal squall lines in spring and mesoscale convective systems (MCSs) in summer [Raubert *et al.*, 2008]. Therefore, it is necessary to collect both in-situ and remotely sensed data with high spatial and temporal resolutions to investigate these

intense and short-lived storm complexes. Similar to the La Niña effect on the U.S. droughts, some studies have suggested teleconnections between the U.S. floods and El Niño events in the Tropical East Pacific (TEP) [e.g., *Trenberth and Branstator*, 1992; *Trenberth and Guillemot*, 1996; *Seager et al.*, 2005]. While considerable efforts have been made to study the droughts and floods, the mechanisms by which extremes can be maintained over multiple years have yet to be established, and relationships between the remote forcing (e.g., TEP sea surface temperatures SSTs) and the response (U.S. extremes) have not been well understood [*Schubert et al.*, 2004a&b; *Seager et al.*, 2005].

The U.S. Great Plains experienced a number of major droughts and floods during the last century, most notably the droughts of 1930s, 1950s and 1988 and the floods of 1993 [*Rauber et al.*, 2008; *Schubert et al.*, 2004a&b; *Seager et al.*, 2005]. During hydrological years 2006 (HY06, 10/01/2005-09/30/2006) and 2007 (HY07, 10/01/2006-09/30/2007), droughts and floods occurred in the U.S. Southern Great Plains (SGP), respectively. The annual and seasonal precipitation amounts and their severities during HY06 and HY07 from the Oklahoma (OK) Climatological Survey are listed in Table 1 and will be discussed in Section 3.1. There are no other examples of two such highly contrasting hydrological extremes occurring in consecutive years, i.e. a dry year followed by a wet year, and no other more comprehensive dataset available in history concerning the droughts and floods at the SGP. This tremendous diversity of observations provides a great opportunity for researchers to investigate the causes of the HY06 drought and HY07 pluvial, and their transitional mechanisms over the SGP region.

To investigate the causes and feedbacks of the two highly contrasting hydrological years, and the impacts of large-scale dynamic and moisture transports from the Gulf of Mexico on these extreme events, we have collected multiple data sets from surface and satellite observations, as

well as reanalyses. These observational results can serve as a baseline for future modeling studies that aim at simulating the onsets/demises of droughts and floods and the multiple feedback processes involved in the formation of these hydrological extremes. The ground-based observations can also serve as ground truth to validate the satellite retrievals, which would promote broad studies of hydrological extremes using satellite retrievals over the regions without the ground-based observations. Through an integrative analysis of observed extremes, we attempt to answer the following four scientific questions in this study:

1. *Are HY06 and HY07 representative of significant drought and pluvial conditions and, if so, how severe and widespread are the effects?*
2. *How do large-scale dynamics play a role in these extreme events?*
3. *To what extent are the severities of the drought and flood affected by cloud and surface energy feedbacks?*
4. *How are these extreme events linked to the moisture transport from the Gulf of Mexico and cyclonic activity?*

## **2. Data**

The data sets listed in Table 2 consist mainly of the Department of Energy (DOE) Atmospheric Radiation Measurement (ARM) [Ackerman and Stokes, 2003] observations at the SGP Central Facility (SCF, 36.6°N, 97.5°W) from January 1997 to December 2007. Other data sets, such as the Oklahoma Mesonet, Version 2 Global Precipitation Climatology Project (GPCP) [Adler *et al.*, 2003], Tropical Rainfall Measuring Mission (TRMM) satellite, National Centers for Environmental Prediction (NCEP) global reanalysis dataset, and the NASA Modern Era Retrospective-Analysis for Research and Applications (MERRA) are also included in this study.

## 2.1 ARM SCF ground-based observations

The ARM observations used in this study include cloud fraction, cumulus (Cu) cloud thickness, cloud liquid water path (LWP), atmospheric column precipitable water vapor (PWV), precipitation, net radiation, sensible (SH) and latent heat (LH) fluxes, and surface air temperature ( $T_{\text{air}}$ ) collected at the ARM SCF during the period 1997-2007. Cloud fraction (CF) is defined by the percentage of returns that are cloudy within a specified sampling period (e.g., a month), i.e., the ratio of the number of hours when radar, lidar and ceilometer all detected clouds simultaneously to the total number of hours when all measurements were available [Dong *et al.*, 2005 and 2006]. Cloud-top height ( $Z_{\text{top}}$ ) is derived from millimeter wavelength cloud radar [MMCR, Moran *et al.*, 1998] reflectivity profiles with the uncertainty of 90 m. Cloud-base height ( $Z_{\text{base}}$ ) is a composite result of Belfort laser ceilometer, Micropluse Lidar (MPL), and MMCR data [Clothiaux *et al.*, 2000]. Cloud physical thickness ( $\Delta Z$ ) is simply the difference between  $Z_{\text{top}}$  and  $Z_{\text{base}}$ . The atmospheric PWV and cloud LWP values are retrieved from the microwave radiometer brightness temperatures measured at 23.8 and 31.4 GHz using a statistical retrieval method [Liljegren *et al.*, 2001]. The root-mean-square (RMS) errors of LWP retrievals are about  $20 \text{ g m}^{-2}$  and 10% for cloud LWP below and above  $200 \text{ g m}^{-2}$ , respectively [Dong *et al.*, 2000; Liljegren *et al.*, 2001].

The surface precipitation is measured by tipping bucket rain gauge at the ARM SCF.  $T_{\text{air}}$  is measured by the conventional in situ sensors (2 m above ground) mounted on a 10-m tower at the ARM SCF site. The SH, LH and net radiation fluxes are measured by the ARM SCF energy balance Bowen ratio system. The SH and LH fluxes are calculated from observations of net radiation, soil surface heat flux, and the vertical gradients of temperature and relative humidity.

## 2.2. Other data sets

To investigate the spatial variations of precipitation, we have also collected the datasets from the Oklahoma (OK) Mesonet system, GPCP, and TRMM over the SGP region. Both GPCP and TRMM data are averaged over a  $5^{\circ}\times 5^{\circ}$  grid box centered on the ARM SCF site. The OK Mesonet is a statewide monitoring network, and consists of over 110 automated weather stations covering the entire state of Oklahoma [Brock *et al.*, 1995]. The OK Mesonet is a system designed to measure the environment at the size and duration of mesoscale weather events.

The monthly GPCP Version 2 precipitation product is used in this study. This product is produced by merging a variety of satellite and ground precipitation measurements, including passive microwave retrievals from SSM/I, infrared-based estimates from geostationary satellites, and gauge observations gridded on  $2.5^{\circ}\times 2.5^{\circ}$  latitude-longitude scale [Adler *et al.*, 2003]. All of the measurements are combined with inverse error variance weighting to produce the merged analysis. In this study, the monthly GPCP data are averaged over a grid box of  $5^{\circ}\times 5^{\circ}$  latitude-longitude covering  $32.5^{\circ}$ - $37.5^{\circ}$ N,  $100^{\circ}$ W- $95^{\circ}$ W during 1997-2007. The TRMM cloud and precipitation products are also averaged over the same grid box as GPCP during 1998-2007. Cloud fraction is derived from a combination of measurements from the TRMM Microwave Imager (TMI) and Visible and Infrared Scanner (VIRS), and precipitation product is the TMI-based TRMM 2A12 rainfall product [Kummerow *et al.*, 2000].

Estimates of radiative heating are obtained from the Hydrologic cycle and Earth's Radiation Budget (HERB) dataset [L'Ecuyer and Stephens, 2003 and 2007]. HERB synthesizes ice cloud microphysical property information from VIRS, liquid cloud properties, precipitation profiles, Sea Surface Temperature (SST), and water vapor retrievals from the TRMM TMI, and vertical profiles of temperature and humidity from European Center for Medium-range Weather



Forecasts (ECMWF) reanalysis, to characterize the three-dimensional structure of clouds and precipitation in the atmosphere. Vertical profiles of SW and LW radiative heating rates are calculated by a broadband radiative transfer model with the input of this dataset [L'Ecuyer and McGarragh, 2010].

The NCEP reanalysis is used to investigate the impact of large-scale dynamics on the two extreme periods. It contains outputs of atmospheric variables and fluxes with 4-times daily temporal resolution,  $2.5^{\circ} \times 2.5^{\circ}$  km horizontal resolution, and 28 vertical levels [Kalnay *et al.*, 1996]. The NASA MERRA reanalysis is also used to quantify the winter cyclonic activity in this study. It contains various 6-hourly atmospheric variables on  $1/3^{\circ} \times 2/3^{\circ}$  grids. Together with the NCEP reanalysis, it provides a comprehensive database for diagnosing synoptic conditions over the SGP and examining their variability on seasonal to longer timescales.

With these ground and satellite observations, the moisture conditions of the two hydrological years can be quantified. The Palmer Drought Severity Index (PDSI) is a popular drought-monitoring tool used by scientists and government agencies to determine extreme weather conditions, such as abnormally wet or abnormally dry periods, as well as their onset and demise [Alley, 1984]. This index is based on the principle of a balance between moisture supply and demand, and takes into account precipitation, evapotranspiration, and soil moisture conditions. That is, the PDSI uses a simple water balance model as basis for developing a regional drought severity index, and does not work for snow or frozen ground. Therefore, caution must be taken when using PDSI index during the snow and frozen months of the year. The PDSI index generally ranges from -6 to +6; with negative values denoting dry spells and positive values indicating wet spells.

### 3. Results and Discussion

In this section, we attempt to address the four scientific questions posed in the beginning. In particular, we will answer question 1 using the NOAA PDSI and four precipitation data sets from ARM, OK Mesonet, GPCP, and TRMM, question 2 using NCEP reanalysis, and question 3 using ARM SCF observations. Finally, by diagnosing both the NASA MERRA reanalysis and TRMM retrievals, we will investigate the linkages between the SGP extremes and the moisture transport from the Gulf Mexico and the winter cyclonic activity.

#### 3.1 Are HY06 and HY07 representative of significant drought and pluvial conditions and, if so, how severe and widespread are the effects?

To study the hydrological extreme events, it is important to have a “benchmark”, or the so-called normal precipitation. The normal precipitation can be a long-term average over a particular area during a certain period (such as over the SGP region in a month in this study). The precipitation anomalies and relative amounts are then calculated against their corresponding normal values. For example, the total of the OK state-mean precipitation during spring 2006 is 23.47 cm, which is about 80% of its normal precipitation. The normal precipitation in this study is the averaged precipitation during 1997-2007 for ARM, OK Mesonet and GPCP, and during 1998-2007 for TRMM over different grid boxes, such as the point for ARM SCF, the entire OK state for OK Mesonet, and  $5^{\circ}\times 5^{\circ}$  for GPCP and TRMM.

Figure 1 shows the monthly state (OK) mean PDSI, four precipitation products and their anomalies and percentages relative to their corresponding averages during the period 1997-2007 (except for TRMM from 1998 to 2007). Notice that the PDSI lags the precipitation by 1-2 months because it has taken into account precipitation, evapotranspiration, and soil moisture

conditions. As demonstrated in Figure 1, moderate drought occurred during the period Feb-June 2005, which is about 40% (the average value from four precipitation datasets) below the normal precipitation, and was then terminated by moderate precipitation during August 2005 (77% above normal). Severe drought started in November 2005 and lasted until February 2006, which is indicated by the roughly 65% below normal precipitation with a maximum deficit of 100%. Thus, we define the period 11/2005-02/2006 as the extreme dry period in this study. Most of 2006 was characterized by persistent dry conditions, slightly below the normal precipitation during fall 2006, and finally changed to a moisture surplus at the end of 2006. In contrast to year 2006, year 2007 was mostly under wet conditions. The period May-July was extremely wet (84% above normal), and a precipitation deficit did not occur until Nov-Dec. 2007. In this study, the two extreme periods (11/2005-02/2006 for extreme dry and May-July 2007 for extreme wet) are selected from four data sets based on the following two criteria: (1) their precipitations were either below or above 50% of their corresponding normal precipitations, and (2) the events lasted at least 3-4 months.

In spite of large spatial and temporal differences among four precipitation products, they all captured the HY06 drought and subsequent HY07 pluvial. Figure 1 also demonstrates that the four precipitation products and their anomalies agree well in both magnitude and sign. This agreement is very encouraging considering that these measurements are made independently by different instruments and the mean precipitations are averaged over different grid boxes and handled by different groups. The good agreement in precipitation between the ARM SCF observations and other three datasets indicates that the point ARM SCF observations can represent a large grid box of observations, at least, up to the size of a 5° grid box during the

studied periods. This result is consistent with those of the cloud fraction comparisons at the ARM SGP site [Xi *et al.*, 2010; Kennedy *et al.*, 2010].

To further investigate the severity and spatial variability of precipitation, we present annual state precipitation anomalies observed by the OK Mesonet for HY06 and HY07 in Figure 2. As shown in Figure 2, the annual state precipitation in HY06 is 31.6 cm below normal, while in HY07 it is 25.1 cm above the 11-yr averaged state precipitation. Oklahoma state experienced statewide drought conditions with a precipitation deficit ( $>40$  cm) over its eastern region during HY06 and pluvial conditions with a precipitation surplus ( $>40$  cm) over its central region during HY07. Therefore, the brief answer to Question 1 is that HY06 and HY07 are indeed significant climatic dry and wet years, respectively. Their severities and ranks are listed in Table 1.

### **3.2. How do large-scale dynamics play a role in these extreme events?**

*Rauber et al.* [2008] discussed the causes of droughts and floods and the role of large-scale dynamics played in controlling these extremes. They found that droughts are normally associated with persistent large-scale flow anomalies, such as those in the subtropical high-pressure system, jet stream, and upper level waves. On the other hand, floods, especially flash floods, are often associated with short-time scale features, such as frontal squall lines and mesoscale convective systems (MCSs). To demonstrate the impact of the large-scale dynamical processes on the HY06 and HY07, especially for the two extreme periods, we plot Figures 3 and 4 using the NCEP reanalysis dataset.

Figure 3 illustrates the means and anomalies (relative to corresponding averages for the period 1979-2007) of 500-hPa geopotential height (GH) during the extreme dry and wet periods. The most prominent feature in Figure 3a is a strong ridge over the Rocky Mountains and a

trough over the Great Lakes. Figure 3c shows a dipole pattern in which an anomalous high is centered over the southwestern U.S. and an anomalous low is over the Great Lakes. This anomalous pattern is favorable for the movement of dry air from Canada southward into the central U.S., restrains the transport of low-level moisture from the Gulf of Mexico. In other words, the northward transport of moist air from the Gulf of Mexico is inhibited. Large-scale vertical motion of air is also a major factor in the occurrence of precipitation where ascending air over a large region favors precipitation and descending air suppresses precipitation. The descending air is adiabatically compressed, which increases the temperature (decreasing relative humidity, RH) and static stability of the atmosphere. The increased static stability and the decreased RH tend to suppress precipitation and lead to drought [McNab and Karl, 2003]. The patterns in Figures 3a and 3c are associated with stronger sinking motion over the SGP relative to the climatology, and contribute to the extreme dryness. The extreme dry period ended during spring 2006 when the large-scale flow pattern over the western U.S. returned to normal (not shown).

For the extreme wet period, Figure 3d illustrates the anomalous high over the northern central U.S. This anomaly is associated with a strong ridge over the Midwest U.S. and is typically indicative of dry conditions over there. South of this ridge, several anomalous lows exist. Inspection of daily synoptic charts revealed that the anomalous low over the TX/OK region was associated with the passage of numerous short-wave troughs in the lee of the Rocky Mountains and a persistent upper-level low. These patterns were associated with rising motion and were conducive to thunderstorm development. Thus the precipitation events during the extreme wet period were initially generated by active weather patterns and enhanced by the

mesoscale convective systems. Local evaporation and feedback processes may help maintain the persistent extremes and enhance their severities as will be discussed in next section.

The 925-hPa RH means and anomalies during the extreme dry and wet periods are plotted in Figure 4. The RH mean over the SGP during the extreme dry period is about 50-60% (Figure 4a), which is about 10% below the corresponding climatological mean RH (Figure 4c). The largest negative RH anomaly ( $\sim -20\%$ ) is located over the southwestern U.S., which corresponds well with the anomalous high shown in Figure 3c. The RH mean over the SGP during the extreme wet period is 80% (Figure 4b), which is approximately 10-20% above the corresponding climatological mean RH (Figure 4d). The region covered by positive RH anomalies (Figure 4d) is much smaller than that covered by negative RH anomalies (Figure 4c), which indicates that the dry area is much larger than the wet area.

As illustrated in Figures 3 and 4, the large-scale dynamical patterns were the major factors that lead to persistent drought during the extreme dry period. The precipitation events during the extreme wet period, however, were initially generated by active weather patterns and enhanced by the mesoscale convective systems. These scattered thunderstorms appeared to enhance and deepen the upper-level low and induce surface low pressure towards the end of June through diabatic processes. As a result, more thunderstorms ensued, and heavy precipitation events persisted for a week at the end of June. The total of OK state mean precipitation during the extreme wet period is approximately 50 cm, including 17 multiple organized convective events and 34 scattered thunderstorms.

### **3.3. To what extent are the severities of the drought and flood affected by cloud and surface energy feedbacks?**

In previous sections, we have demonstrated that HY06 and HY07 are indeed under significant drought and pluvial conditions, respectively, and dominated by large-scale dynamic patterns. However, it is unclear to what extent these extreme events are associated with the seasonal variations of cloud properties and surface energy, and affected by cloud and surface energy feedbacks. Further, what phase relationships exist between the cloud and surface properties? For variables that have either leading or lagging relationships each other, what does this imply about maintaining and reinforcing drought and pluvial conditions?

To answer these questions, we present the monthly means (Figs. 5&6) of CF, cumulus (Cu) cloud thickness (contiguous clouds, cloud base<3 km and cloud top>6 km), cloud LWP, atmospheric PWV, precipitation, net radiation, SH, LH, and  $T_{\text{air}}$  at the ARM SCF during the HY06, HY07, and 11-yr climatological periods. To investigate the phase relationships among the variables, we list their correlations (in phase, one-month lead, and one-month lag) in Tables 3a and 3b based on their monthly means and anomalies, respectively, during the period 10/2005-09/2007. Finally, we discuss to what extent the extreme events are enhanced by the cloud and surface energy feedbacks at the end of this section.

As illustrated in Fig. 5, the CFs in HY06 and HY07 are 0.056 lower and 0.032 higher than the 11-yr mean, respectively. The CFs during the two extreme periods are 0.138 below and 0.203 above their corresponding 11-yr averages, respectively. The average Cu cloud thickness in HY06 is about 0.44 km thinner than the 11-yr mean, and is 0.93 km thinner for the extreme dry period. The average Cu cloud thickness in HY07, however, is 1.32 km thicker than the 11-yr mean, and is 1.946 km thicker for the extreme wet period. The monthly mean LWPs during HY06 are consistently lower than the 11-yr means, and the annual average LWP in HY06 is only 43% of the 11-yr mean LWP. While the average LWP in HY07 is slightly larger than the 11-yr

mean, the average LWP during the extreme wet period is double the 11-yr average (628 vs. 306  $\text{gm}^{-2}$ ). The total precipitation is 2.32 cm (vs. 21.68 cm of 11-yr average) during the extreme dry period, and is 58 cm (vs. 32 cm of 11-yr average) for the extreme wet period. The precipitation has moderate correlations with CF and PWV (0.6 and 0.49), and relatively high correlations with Cu thickness and LWP (0.74 and 0.844). As listed in Table 3a, these correlations are significant at a 99% confidence interval (CL) except for PWV at a 95% confidence level.

Figure 5d and Figures 6a&6b have demonstrated that there are strong seasonal variations in atmospheric PWV, net radiation and  $T_{\text{air}}$  where they increase monotonically from winter to summer from 11-yr averages. More solar radiation absorbed by the ground during summer results in increased  $T_{\text{air}}$  and atmospheric PWV, which is supported by the high correlations between  $T_{\text{air}}$  and net radiation (0.893) and PWV (0.916) in Table 3a. The seasonal variation of SH mirrors the variations in PWV, net radiation and  $T_{\text{air}}$  (Correlations= -0.681, -0.851, and -0.723), but it peaks (negative values represent that the ground is warmer than the air above and heat is transferred upwards into the air) one-month earlier (in June) than those of PWV, net radiation and  $T_{\text{air}}$ . This result suggests that most of net radiation ( $129.5/163.5=79.2\%$ ) was transferred upwards into the air from the ground in June. These correlations are significant at a 99% confidence interval. There is also seasonal variation in LH, but it is not as strong as other variables. The LH values are comparable to the SH values from late fall to early spring, but are much smaller than the SH values from late spring to early fall (30% LH vs. 70% SH).

Surface air temperature  $T_{\text{air}}$  is determined by the sum of the net radiative (SW and LW fluxes) and nonradiative fluxes [SH+LH, ground heat is much smaller than SH and LH] [Wild *et al.*, 2004]. Although the sum of annual mean SH, LH and net radiation is nearly zero ( $+1.6 \text{ Wm}^{-2}$ ) during 11-yr period, the sums of their monthly means are negative from October to February



(the ground lost energy) and positive from April to September (the ground gained energy). This is consistent to the seasonal variation of  $T_{\text{air}}$  with a minimum of 276 K in January-February, and a maximum of 300 K in July-August as shown in Figure 6. The sum of annual mean SH, LH, and net radiation is nearly balanced ( $-2.1 \text{ Wm}^{-2}$ ) in HY06, while it is  $-9.1 \text{ Wm}^{-2}$  in HY07, indicating that the ground lost more energy during HY07. During the extreme wet period, the averaged net radiation, SH and LH are 141.4, -127.2, and  $-30.2 \text{ Wm}^{-2}$  (the sum= $-16 \text{ Wm}^{-2}$ ), respectively, while their corresponding averages during 11-yr period are 161.4, -118.6, and  $-32.1 \text{ Wm}^{-2}$  (the sum= $10.7 \text{ Wm}^{-2}$ ). The  $26.7 \text{ Wm}^{-2}$  energy loss results in  $-1.1 \text{ K}$   $T_{\text{air}}$  decrease. The SW flux absorbed at the surface is  $29 \text{ Wm}^{-2}$  lower than its corresponding average due to more CF, LWP, and precipitation.

As listed in Table 3a, the correlations between precipitation and cloud properties for phase differences of one-month lead and lag are much smaller than those for the same month, indicating that precipitation and cloud properties are general in-phase. However, there are some phase delays between surface properties and atmospheric PWV as reflected by their higher correlations for one-month earlier/late than those in the same month. For example, the correlations between PWV and net radiation/SH in one-month late, and between net radiation/SH and  $T_{\text{air}}$  in one-month earlier are higher than those in the same month, suggesting that the net radiation and SH in previous month play a key role for the following month of atmospheric PWV and surface air temperature. Generally, monthly temperature change lags that of net radiation, especially solar radiation, about a month with  $\text{CL} > 99\%$ .

The correlations calculated from monthly means may represent both the seasonal variations of variables and the relationships among the variables. The correlations calculated from the monthly anomalies which removed the seasonal variations may represent the real relationships

among the variables and are provided in Table 3b. Comparing the two tables, we find that the correlations between precipitation and cloud property anomalies are close to or slightly lower than those from monthly means, and the correlation between precipitation and PWV anomalies are higher. This comparison demonstrates that there are indeed some relationships between the precipitation and cloud properties during the period 10/2005-09/2007 with  $CL > 99\%$ . For the surface property anomalies, most of their correlations are much lower than those from monthly means with  $CL < 95\%$ , indicating that these variables basically follow the seasonal variations. We also calculate the correlations from the 11-yr monthly anomalies (not shown), and find that their correlations and confidence levels are much lower than those from the 2-yr period. This comparison suggests that the relationships among the variables and feedback processes during HY06 and HY07 were much stronger than those from 11-yr period.

Radiative flux anomalies derived from TRMM observations tend to agree very well with those presented in Fig. 6. The HERB dataset can, therefore, be used to extend the localized SGP measurements to the larger domain from  $33\text{--}38^\circ\text{N}$  and  $95\text{--}100^\circ\text{W}$  encompassing the area of strongest precipitation anomalies in Fig. 2. These data are used to explore the response of atmospheric radiative heating rates ( $>0$  for heating and  $<0$  for cooling) to drought/flood events in the SGP region in Fig. 7. Monthly anomalies from October 2005 through December 2007 (relative to the averages for 1998-2007) of raining, low, high, and total cloud fractions, as well as the NET, SW and LW heating profile anomalies over the broader SGP region suggest that, similar to their precipitation counterpart, fewer clouds occurred over the SGP during HY06 while clouds were more prevalent than normal in subsequent HY07.

During the extreme wet period, increased high clouds led to a marked increase in SW heating from 6 to 12 km and a reduction of SW radiation that reached lower levels relative to the

11-year mean for the region, consistent with SW fluxes measured at the ARM SCF. This reduction offsets the increased SW heating due to increased low-level clouds. In the meantime, increased high clouds lead to enhanced LW heating at cloud base and LW cooling near cloud top. The increased downward LW heating warms low and middle clouds and offsets the increased LW cooling due to the increased low and middle clouds. Therefore, the overall net (SW+LW) effect due to the increased clouds during the extreme wet period is the heating of the atmosphere from the surface up to 10 km.

Although not as strong as the extreme wet period, an opposite signature was found during the 2006 drought period with reduced SW heating aloft, increased SW heating near the surface, and anomalously strong LW cooling from the surface to 6 km (allowing more emission from the lower atmosphere to escape to space) with a net effect of cooling the atmosphere. Thus changes in cloudiness act to decrease atmospheric stability locally during the wet period while stabilizing the atmosphere during the dry period. While it is very unlikely that these local effects play a first-order role in the persistence of droughts or floods they have the potential to impact future precipitation development in the region in a way that would tend to reinforce existing drought or pluvial conditions.

In Figures 5-7, we have demonstrated that there are strong seasonal variations in atmospheric PWV, net radiation, SH, and  $T_{\text{air}}$ ; and precipitation is positively correlated with CF, cumulus cloud thickness, and LWP. However, it is unclear to what extent the extreme events are enhanced by the cloud and surface energy feedbacks during the two extreme periods. Based on the previous studies [e.g., *Rauber et al.*, 2008], these feedbacks are normally positive, i.e., reinforcing or enhancing an existing drought or flood event, or making dry areas drying and wet

areas wetter. In this study, we will demonstrate the two positive feedback processes during the extreme dry and wet periods based on the ARM SCF observations.

During the extreme dry period, more net radiation (compared to 11-yr mean) was absorbed by the ground ( $+4.1 \text{ Wm}^{-2}$ ), which resulted from less clouds ( $-0.138$ ), cloud LWP ( $-193 \text{ gm}^{-2}$ ), and precipitation ( $-4.59 \text{ cm}$ ), as well as thinner Cu cloud thickness ( $-0.929 \text{ km}$ ). The absorbed net radiation by the ground is mostly ( $\text{LH} = -27.9$  vs. 11-yr mean  $= -23.3 \text{ Wm}^{-2}$ ;  $62.3\%$  vs.  $55.2\%$  for the 11-yr mean) used to evaporate water from the ground. Because of the favorable large-scale dynamic conditions, the evaporated moisture was removed from the dry region by low-level divergence as demonstrated in Fig. 3c and weakly southward low level jet (will be discussed in next section). Thus, with less precipitation during the extreme dry period and removed atmospheric moisture, more absorbed incoming solar radiation was used to increase  $T_{\text{air}}$  ( $0.92 \text{ K}$ ) and to make the ground drier. This result is consistent to the findings in Figure 7 where the heating rate anomalies in the lower atmosphere during HY06 are negative (due to drier atmosphere, less cloud and precipitation) than normal year. This feedback process is also valid for the entire HY06 period as illustrated in their annual means in Figures 5-6. These results demonstrate a positive feedback mechanism, which provides a physical basis for interpreting the observed tendency of a drought to “feed upon itself” as mentioned in *Rauber et al.* [2008].

During the extreme wet period, more precipitation ( $+8.66 \text{ cm}$ ) is strongly associated with increased PWV ( $+0.426 \text{ cm}$ ), CF ( $+0.203$ ), cloud LWP ( $+322 \text{ gm}^{-2}$ ), and thicker Cu cloud thickness ( $+1.946 \text{ km}$ ), but with decreased net radiation ( $-20 \text{ Wm}^{-2}$ ) and surface temperature ( $-1.11 \text{ K}$ ). The averaged sum of net radiation, SH, and LH is  $-16 \text{ Wm}^{-2}$ , indicating that more heat (SH) is transferred upwards from the ground to warm the lower atmosphere. This result is consistent to the positive heating rate anomalies of the atmosphere during the extreme wet period

as illustrated in Fig. 7. The averaged LH value during the extreme wet period is nearly the same as that of 11-yr period, varying from below (more negative) to above (less negative) the 11-yr averages for the period of May to July. With more precipitation in May 2007, more surface energy is transferred upwards as evaporation which is one of the reasons of increased PWV. This process, as mentioned previously, could make local convection much easier and result in more precipitation later on (in June).

However, this positive feedback process is not as straightforward as the extreme dry period (a persistent and abnormal moisture deficiency over a particular area) because one heavy precipitation event could destroy the previous balance. The increased PWV may be attributed from local evaporation (LH values) and moisture transports, especially from the Gulf of Mexico by the low level jet (LLJ). As shown in Table 3a, the atmospheric PWV has a strong positive correlation with net radiation (0.844) and moderate negative correlations with SH and LH fluxes (-0.681 and -0.435), however, PWV lags the net radiation and SH a month as demonstrated in their higher correlations (0.924 and -0.834). This makes a physical sense because increased net radiation results in high temperature and SH, and thereafter leads to the increases in saturated vapor pressure of the atmosphere. Later on, when local meteorological conditions transfer to a state favorable rainfalls like the extreme wet events, the atmospheric moisture and local convection increase, which enhances the precipitation.

Although the drought and pluvial conditions are dominated by large-scale dynamic patterns, we have demonstrated that the two positive feedback processes during the extreme dry and wet periods found in this study play a key role to maintain and reinforce the length and severity of existing drought and flood events. More detailed modeling studies and extensive analyses of multiple events would be required to validate these feedback processes and further

understand their maintenance mechanisms. In the mean time, moisture transport from the Gulf of Mexico by LLJ and the Western Pacific (WP) teleconnection pattern are still likely the most important factors governing the length and severity of the SGP droughts and/or floods.

### **3.4 How are these extreme events linked to the moisture transport from the Gulf of Mexico and cyclonic activity?**

As discussed in previous section, the PWV over the ARM SCF may be attributed from both local evaporation and also moisture transport from the Gulf of Mexico by LLJ. To demonstrate the relationships between these extreme events and moisture transport from the Gulf of Mexico, we show a time series of the meridional component of the vertically integrated moisture transport from the Gulf of Mexico (positive for northward) during HY06, HY07 and 9-yr period in Figure 8 and the 900-hPa meridional wind (LLJ) during May-July 2007 in Figure 9. The moisture transport averaged over 97°W–90°W across 28°N in the Gulf of Mexico was derived from the surface wind vector from NASA’s QuikSCAT, NOAA’s cloud drift winds, and integrated water vapor from SSM/I, using a statistical model [Xie *et. al.*, 2008]. Figure 8 shows that there are less (-8.5%) moisture transport in HY06 and more (+8.1%) in HY07 than the average of 1999-2007. The moisture transports during the extreme dry and wet periods are 84.7% and 112.6% relative to their corresponded 9-yr averages, indicating much less moisture transport during the extreme dry period and HY06, and much more moisture transport during the extreme wet period and HY07 than normal years.

The Great Plains Low Level Jet (GPLJJ) is well known for its importance of northward moisture transport from the Gulf of Mexico, which provides both the thermodynamic and dynamic environment to aid in precipitation formation over the Great Plains. Although LLJ is

typically nocturnal, its strength and frequency are large enough for it to manifest itself during the spring and summer on a monthly scale [Stensrud, 1996]. Weaver et al. [2008] found that GPLJJ variability can be reasonably characterized by the averaged 900-hPa meridional wind from NECP reanalysis. This variability has moderate correlations with precipitation that are strongest during the months of June and July.

The LLJ means and anomalies during the extreme dry and wet periods have been investigated for their presence. The LLJ directions could be both southward and northward during the winter months (not shown) with a neutral average ( $\sim 0 \text{ ms}^{-1}$ ) from 29 years of NCEP reanalysis. Therefore, moisture from the Gulf of Mexico has generally minimal influence on precipitation and wintry storms over the SGP region during winter months. During the extreme dry period, there were only weak ( $\sim -0.5 \text{ ms}^{-1}$ , southward) anomalies over portions of OK and southern Kansas. Thus, the droughts during the extreme dry period had some influences from the weakly southward LLJ and slightly reduced moisture transport from the Gulf of Mexico. During the extreme wet period, however, the monthly LLJ means and anomalies were much large as demonstrated in Figure 9. For all three months, the GPLJJ means appeared as the ribbon of southerly winds extending from the Gulf of Mexico to Dakotas with peaks of  $\sim 10 \text{ ms}^{-1}$  during June. During May (Fig. 9d), the LLJ anomaly was slightly stronger ( $2 \text{ ms}^{-1}$ ) than the average of 1979-2007 over the ARM SCF. During June, the LLJ anomaly was also slightly stronger with a dipole of  $\sim 2 \text{ ms}^{-1}$  meridional wind existed over the southwest of OK (Fig. 9e). This dipole pattern is in agreement with the persistent low pressure system over the SGP region during this month as discussed at the end of Section 3.2. For July (Figs. 9c and 9f), both GPLJJ mean and anomaly were much weak with negative anomalies on order of  $-1$  to  $-2 \text{ ms}^{-1}$  throughout the SGP region.

Based on the results of Figures 8 and 9, we draw the following conclusion for moisture transport from May to July 2007. During May, the LLJ is primarily strong over the Northern Great Plains, and its moisture transport from the Gulf of Mexico to the SGP is below normal (Fig. 8). For July, the transported moisture should be near or just below normal at the SGP due to a weak LLJ, despite high values of moisture transport at 28° N. During June, however, the transported moisture is higher than normal because of the strong LLJ and/or persistent low pressure system. This conclusion provides a strong support to the findings of Figures 5 and 6 at the ARM SCF, such as the heaviest precipitation during June 2007.

The extreme dry period is characterized by a large precipitation deficit during the 2005-2006 winter months (Table 1). Since the SGP winter precipitation is typically associated with the passage of extratropical cyclones [Rauber *et al.*, 2008], it is important to examine the anomalous activity of these synoptic-scale, precipitation-producing systems during winter months. Understanding the connection between this anomalous cyclonic activity and large-scale teleconnection patterns helps to infer potential predictability of winter hydrological extremes over the SGP region. Here we quantified the cyclonic activity in 30 winters (Nov-Feb, 1979/80-2008/09) by computing the accumulated daily negative 300-hPa GH anomalies (i.e., 300-hPa short-wave troughs) based upon the NASA MERRA data. The “feature tracking” method of Hoskins and Hodges [2002] was adopted to detect and track the synoptic-scale GH anomalies over 6-hour intervals.

Figure 10a shows the correlation between the monthly cyclonic activity over the continental U.S. and the precipitation over a grid box of 30-40°N and 105-95°W representing the broader SGP region during the period Nov-Feb., 1979/80-2008/09 (please note that the sign of precipitation was reversed in the calculation to reflect the drought condition). The winter



precipitation deficit over the SGP is clearly linked to significantly suppressed cyclonic activity (i.e., negative anomalies) over the southwestern U.S. This result is consistent with a winter cyclone's westward-tilt with height, thus the fact that the surface precipitation zone tends to be located to the east of the upper-level (300-hPa) trough. The suppressed cyclonic activity (Fig. 10b) and positive 500-hPa GH anomalies (Fig. 3c) over the southwestern U.S. have demonstrated that large-scale flow anomalies play a key role in leading to this extreme dry period.

To find out what teleconnection patterns can modulate the cyclonic activity over the southwestern U.S. and therefore drive the winter precipitation variability in the SGP, we first defined a Cyclonic Activity Index (CAI) by integrating anomalies of the cyclonic activity over 30-37°N and 120-100°W representing the southwestern U.S. The correlation coefficients between this index and the Northern Hemisphere (NH) 500-hPa GH were given in Figure 11a where enhanced cyclonic activity in winter is generally associated with positive (negative) height anomalies over the western Pacific regions south (north) of Japan and negative height anomalies over the southwestern U.S. The suppressed cyclonic activity during the extreme dry period thus corresponds to the exact opposite of the anomalous pattern shown in Fig. 11a. This triple-action-center pattern clearly resembles the loading pattern of the Western Pacific (WP) teleconnection, a primary low-frequency mode over the North Pacific [Wallace and Gutzler, 1981; Barston and Livezey, 1987]. In fact, the correlation between the Nov-Feb averaged CAI and the WP index is 0.43 and statistically significant at the 99% level (Fig. 11c). The southwestern CAI is also slightly correlated with the Pacific-North America (PNA) index on monthly time scales with a correlation coefficient of 0.21 statistically significant at the 95% level (Fig. 11b). Since positive phases of WP and PNA are characterized by negative GH anomalies over the western North

America and the North Pacific respectively, and such anomalies tend to push westerly jets southward and enhance upper level divergence downstream of the GH anomalies, the positive phases of WP and PNA can contribute to increased cyclonic activity over the Southwest. This is consistent with the positive correlations between the CAI and WP/PNA identified above. Given the linkages between the CAI (therefore, the SGP precipitation) and the WP and PNA index on respectively seasonal and monthly time scales, improved understanding and simulation of the WP and PNA variability have strong implications for future studies that explore the predictability of the SGP winter hydrological extremes.

#### **4. Summary and conclusions**

In this study, we analyze the comprehensive datasets collected at the ARM SCF site during HY06 and HY07, the two most highly contrasting extreme hydrologic years occurring in consecutive in the SGP in history. The tremendous diversity of observations during these two years provides a great opportunity for researchers to investigate the contrast between drought and flood, and the transitional mechanisms at the SGP region, which may lead to new insights into the factors that lead to persistent drought and flooding. Through an integrative analysis of observed extremes, we briefly answer the four scientific questions posed in the beginning as follows:

- 1) HY06 and HY07 are indeed significant climatological dry and wet years, respectively. The HY06 annual precipitation (over the entire state of Oklahoma) observed by the OK Mesonet is only 61% of the normal (92.84 cm, average from 1921 to 2008) and HY06 ranks as the second-driest year on record since 1921. For the seasonal variation, the state mean precipitation (3.7 cm) during the winter of 2005-06 is only 27% of the normal and this winter ranks as the driest season

in the record. The HY07 annual precipitation is 21% above the normal and HY07 ranks as the seventh-wettest year for the entire state and the wettest year for the central region. Summer 2007 is the second-wettest season for the entire state with a total precipitation of 40.8 cm (68% higher than the normal).

2) Large-scale dynamics play a key role in these extreme events. During the extreme dry period, a dipole pattern in the 500-hPa GH anomaly existed where an anomalous high was over the southwestern U.S. region and an anomalous low was over the Great Lakes. This pattern was associated with inhibited moisture transport from the Gulf of Mexico and strong sinking motion over the SGP, both contributing to the extreme dryness. The precipitation events during the extreme wet period were initially generated by the passages of short-wave troughs in the lee of the Rocky Mountains and a persistent upper low, and enhanced by the frequency of thunderstorms and their associated latent heat release.

3) Based on the ARM SCF observations, we find that the precipitation has moderate correlations with CF and PWV, and relatively high correlations with Cu thickness and LWP. There are strong seasonal variations in atmospheric PWV, net radiation and  $T_{\text{air}}$  where they increase monotonically from winter to summer. The seasonal variation of SH mirrors the variations in PWV, net radiation and  $T_{\text{air}}$ , but it peaks one month earlier than those of PWV, net radiation and  $T_{\text{air}}$ . The LH values are comparable to the SH values from late fall to early spring, but much smaller than the SH values from late spring to early fall (30% LH vs. 70% SH). Generally, precipitation and cloud properties are in-phase, however, temperature change lags that of net radiation, especially solar radiation, about a month with  $CL > 99\%$ .

Although the drought and pluvial conditions are dominated by large-scale dynamic patterns, we have demonstrated that the two positive feedback processes during the extreme dry and wet

periods play a key role to maintain and reinforce the length and severity of existing drought and flood events. During the extreme dry period, with less clouds, LWP, PWV, precipitation, and thinner Cu cloud thickness, more net radiation was absorbed and used to evaporate water from the ground. The evaporated moisture, however, was removed by low-level divergence. Thus, with less precipitation and removed atmospheric moisture, more absorbed incoming solar radiation was used to increase surface temperature and to make the ground drier. During the extreme wet period, more precipitation is strongly associated with increased CF, LWP, PWV, and thicker Cu cloud thickness, but with decreased net radiation and surface temperature. The precipitation events during the extreme wet period were initially generated by active weather patterns and enhanced by the mesoscale convective systems.

4) The transported moisture from the Gulf of Mexico and the cyclonic activity are certainly important to these extreme events. There were less and more moisture transports during HY06 and HY07, respectively. The droughts during the extreme dry period had some influences from the weakly southward LLJ and slightly reduced moisture transport from the Gulf of Mexico. During the extreme wet period, however, their LLJ means and anomalies were large and their values of moisture transport were high. These results have demonstrated that the precipitation events over the SGP region, especially in June 2007, are definitely linked with strong LLJ and high moisture transport from the Gulf of Mexico. From the synoptic perspective, the winter precipitation deficit over the SGP is clearly linked to significantly suppressed cyclonic activity over the southwestern U.S. where it is modulated by winter atmospheric low-frequency modes over the Pacific such as the WP and PNA teleconnection patterns.

By contrasting HY06 drought with HY07 flooding and highlighting their major difference in terms of precipitation statistics, cloud properties, surface energy and large-scale flow patterns,

this investigation provides an integrated dataset for hydrological studies over the U.S. SGP during the period 1997-2007. These observational results can provide constraints and ground truth for modelers to improve their simulations. For example, we use two WRF microphysical schemes for a case study with and without graupel, and their simulated precipitations are close to and higher than observations, respectively. Although we have quite successfully answered the posed four questions, many overlying issues still remain. For example, how can we build upon this regional study, and devise observational strategy and diagnostic tool to explore hydrological extremes on a continental or global scale? To what extent are these extremes and processes predictable and on what time scales? Ongoing and future modeling work will lend more insights into the factors that control the persistence and intensity of droughts and floods, and explore the predictability of these extremes over the SGP and other climate regimes.

#### ***Acknowledgements:***

Surface Data and Oklahoma Mesonet precipitation were obtained from the Atmospheric Radiation Measurement (ARM) Program sponsored by the U.S. Department of Energy (DOE) Office of Energy Research, Office of Health and Environmental Research, Environmental Sciences Division. This research was primarily supported by NASA Energy and Water Cycle Study (NEWS) project that managed by Dr. Jared Entin. The University of North Dakota authors were supported by NEWS project under Grant NNX07AW05G, and supported by NASA CERES project under Grant NNL04AA11G. The Georgia Institute of Technology authors were supported by NASA NEWS under Grant NNX09AJ36G.

## References

- Ackerman, T. P., and G. M. Stokes, The Atmospheric Radiation Measurement Program, *Phys. Today*, 56, 38-44, 2003.
- Adler, R.F., G.J. Huffman, A. Chang, R. Ferraro, P. Xie, B. Rudolf, U. Schneider, S. Curtis, D. Bolvin, A. Gruber, J. Susskind, P. Arkin, and E. Nelkin, The Version 2 Global Precipitation Climatology Project (GPCP) Monthly Precipitation Analysis (1979-Present), *J. of Hydrometeorol.*, 4, 1147-1167, 2003.
- Alley, W.M., The Palmer Drought Severity Index: Limitations and assumptions, *J. of Clim. Appl. Meteorol.*, 23, 1100–1109, 1984.
- Brock, F.V., K.C. Crawford, R.L. Elliott, G.W. Cuperus, S.J. Stadler, H.L. Johnson, and M.D. Eilts, The Oklahoma Mesonet: A Technical Overview, *J. Atmos. Oceanic Technol.*, 12, 5–19, 1995.
- Clothiaux, E.E., T.P. Ackerman, G.G. Mace, K.P. Moran, R.T. Marchand, M.A. Miller, and B.E. Martner, Objective determination of cloud heights and radar reflectivities using a combination of active remote sensors at the Atmospheric Radiation Measurement Program Cloud and Radiation Test Bed (ARM CART) sites, *J. Appl. Meteorol.*, 39, 645-665, 2000.
- Dong, X., P. Minnis, T.P. Ackerman, E.E. Clothiaux, G.G. Mace, C.N. Long, and J.C. Liljegren, A 25-month database of stratus cloud properties generated from ground-based measurements at the ARM SGP site, *J. Geophys. Res.*, 105, 4529-4538, 2000.
- Dong, X., P. Minnis, and B. Xi, A climatology of midlatitude continental clouds from ARM SGP site. Part I: Low-level Cloud Macrophysical, microphysical and radiative properties, *J.*

689       *Clim.*, 18, 1391-1410, 2005.

690   Dong, X., B. Xi, and P. Minnis, A climatology of midlatitude continental clouds from the ARM

691       SGP Central Facility: Part II: Cloud fraction and surface radiative forcing, *J. Clim.*, 19,

692       1765-1783, 2006.

693   Hoskins, B.J., and K.I. Hodges, New Perspectives on the Northern Hemisphere Winter Storm

694       Tracks, *J. Atmos. Sci.*, 59, 1041–1061, 2002.

695   Kalnay, E., and coauthors, The NCEP/NCAR 40-year reanalysis project, *Bull. Am. Meteorol.*

696       *Soc.*, 77, 437-470, 1996.

697   Kennedy, A., X. Dong, B. Xi, P. Minnis, A.D. Del Genio, and A.B. Wolf, Evaluation of the

698       NASA GISS Single Column Model Simulated Clouds Using Combined Surface and

699       Satellite Observations, Accepted by *J. Clim.*, 2010.

700   Kummerow, C. D. and coauthors, The status of the Tropical Rainfall Measuring Mission

701       (TRMM) after two years in orbit, *J. Appl. Meteorol.*, 39, 1965-1982, 2000.

702   L'Ecuyer, T. S. and G. L. Stephens, The Tropical Oceanic Energy Budget from the TRMM

703       Perspective. Part I: Algorithm and Uncertainties, *J. Clim.*, 16, 1967-1985, 2003.

704   L'Ecuyer, T. S. and G. L. Stephens, The tropical atmospheric energy budget from the TRMM

705       perspective. Part II: Evaluating GCM representations of the sensitivity of regional energy

706       and water cycles to the 1998-99 ENSO cycle, *J. Clim.*, 20, 4548-4571, 2007.

707   L'Ecuyer, T. S. and G. McGarragh, A 10-year climatology of tropical radiative heating and its

708       vertical structure from TRMM observations, *J. Clim.*, 519-541, 23, 2010.

709   Liljegren, J. C., E.E. Clothiaux, G.G. Mace, S. Kato, and X. Dong, 2001: A new retrieval for

710       cloud liquid water path using a ground-based microwave radiometer and measurements of

711       cloud temperature, *J. Geophys. Res.*, 106, 14,485-14,500, 2001

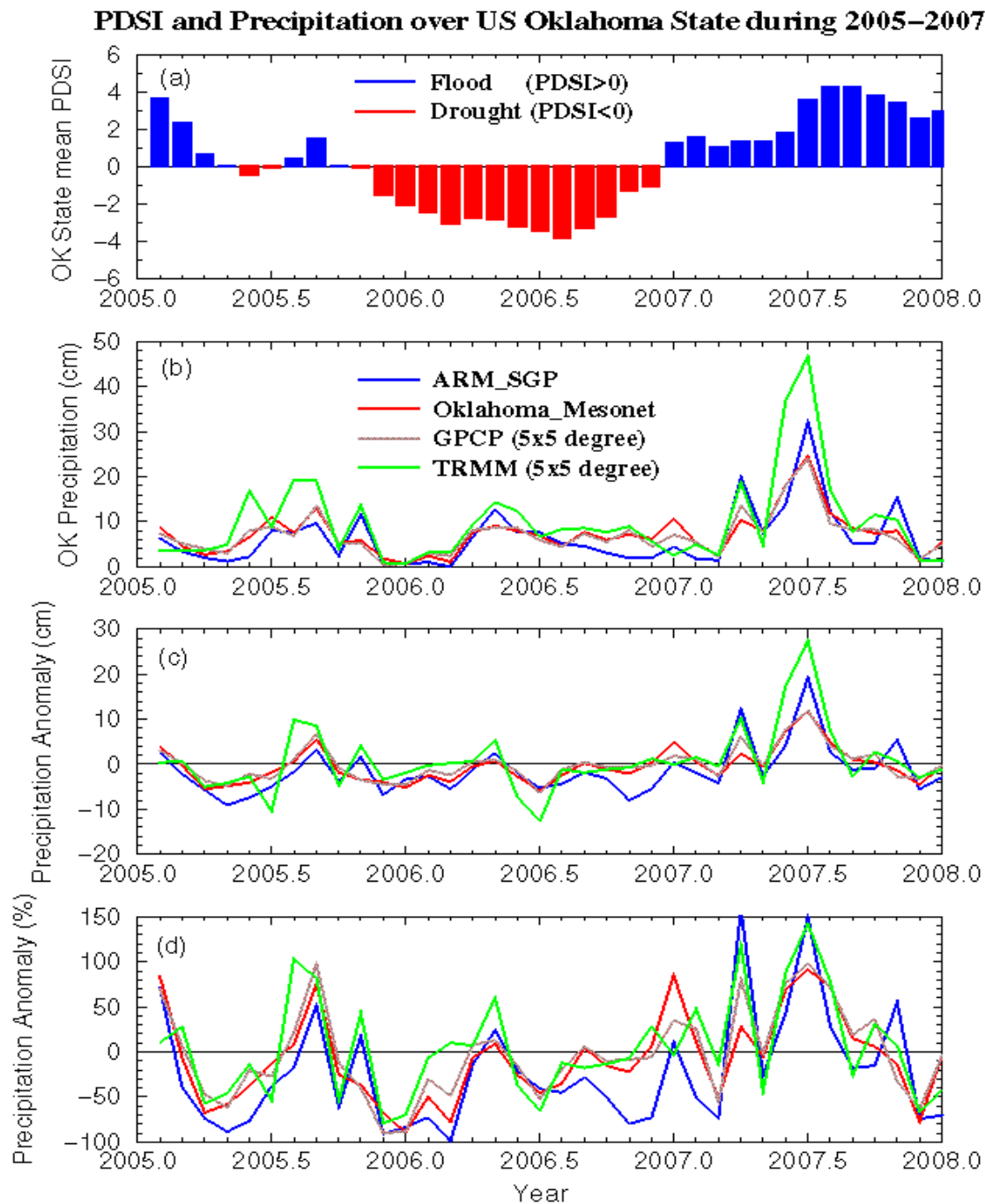
712 Long, C. N., and Y. Shi, An automated quality assessment and control algorithm for surface  
 713 594 radiation measurements, *J. of the Open Atmos. Sci.*, 2, 23-37, 2008.  
 714 McNab. A.L., and T.R. Karl, Climate and Droughts. Available at  
 715 <http://geochange.er.usgs.gov/sw/changes/natural/drought/>, 2003.  
 716 Moran, K.P., B.E. Martner, M.J. Post, R.A. Kropfli, D.C. Welsh, and K.B. Widener, An  
 717 unattended cloud-profiling radar for use in climate research, *Bull. Am. Meteorol. Soc.*, 79,  
 718 443-455, 1998.  
 719 Namias, J., Multiple causes of the North American abnormal winter 1976-77, *Mon. Weather*  
 720 *Rev.*, 106, 279-295, 1978.  
 721 Rauber, R.M., J.H. Walsh, and D. J. Charlevoix, Severe and Hazardous Weather, Kendall/Hunt  
 722 Publishing company, 3<sup>rd</sup> version, P642, 2008.  
 723 Schubert, S.D., M.J. Suarez, P.J. Pegion, R.D. Koster, and J.T. Bacmeister, Causes of Long-  
 724 term Drought in the U.S. Great Plains, *J. Clim.*, 17, 485-503, 2004a.  
 725 Schubert, S.D., M.J. Suarez, P.J. Pegion, R. D. Koster, and J.T. Bacmeister, On the Cause of the  
 726 1930s Dust Bowl, *Science*, 303, 1855-1859, 2004b.  
 727 Seager, R., Y. Kushnir, C. Herweijer, N. Naik, and J. Velez, Modeling of Tropical Forcing of  
 728 Persistent Droughts and Floods over Western North America: 1856-2000, *J. Clim.*, 18, 4065-  
 729 4088, 2005.  
 730 Stensrud, D. J., 1996: Importance of low-level jets to climate: A review. *J. Clim.*, 9:1698–1711.  
 731 Trenberth, K.E., and G.W. Branstator, Issues in Establishing Causes of the 1988 Drought over  
 732 North America, *J. Clim.*, 5, 159-172, 1992.  
 733 Trenberth, K.E., and C. J. Guillemot, Physical Processes Involved in the 1988 Drought and 1993  
 734 Floods in North America, *J. Clim.*, 9, 1288-1298, 1996.



- UCAR, Understanding Drought. Available at the UCAR COMET® Website at <http://meted.ucar.edu/>, 2009.
- Wallace, J.M., and D.S. Gutzler, Teleconnections in the Geopotential Height Field during the Northern Hemisphere Winter, *Mon. Weather Rev.*, *109*, 784–812, 1981.
- Weaver, S. J. and S. Nigam, 2008: Variability of the Great Plains low-level jet: Large-scale circulation context and hydroclimate impacts. *J. Clim.*, *21*:1532–1551.
- Wild, M., A. Ohmura, H. Gilgen, and D. Rosenfeld, On the consistency of trends in radiation and temperature records and implications for the global hydrological cycle, *Geophys. Res. Lett.*, *31*, L11201, doi:10.1029/2003GL019188, 2004.
- Xi, B., X. Dong, P. Minnis, and M. Khaiyer, A 10-year climatology of cloud cover and vertical distribution derived from both surface and GOES observations over the DOE ARM SGP Site, *J. Geophys. Res.*, in press, 2010.
- Xie, X., W.T. Liu and B. Tang, Spacebased estimation of moisture transport in marine atmosphere using support vector machine, *Remote Sens. Environ.*, *112*, 1845-1855, 2007.

758

759



760

761

762

Figure 1. (a) Monthly mean PDSI over Oklahoma state, (b) monthly accumulated precipitations measured at the DOE ARM SCF site, over the entire state measured by Oklahoma mesonet

system, and over a 5°x5° grid box (32.5-37.5°N, 100-95°W) derived from GPCP and TRMM observations. (c) and (d) are the same as (b) but for the monthly anomaly values and percentages (relative to corresponding averages for the period 1997-2007 except for TRMM from 1998-2007).

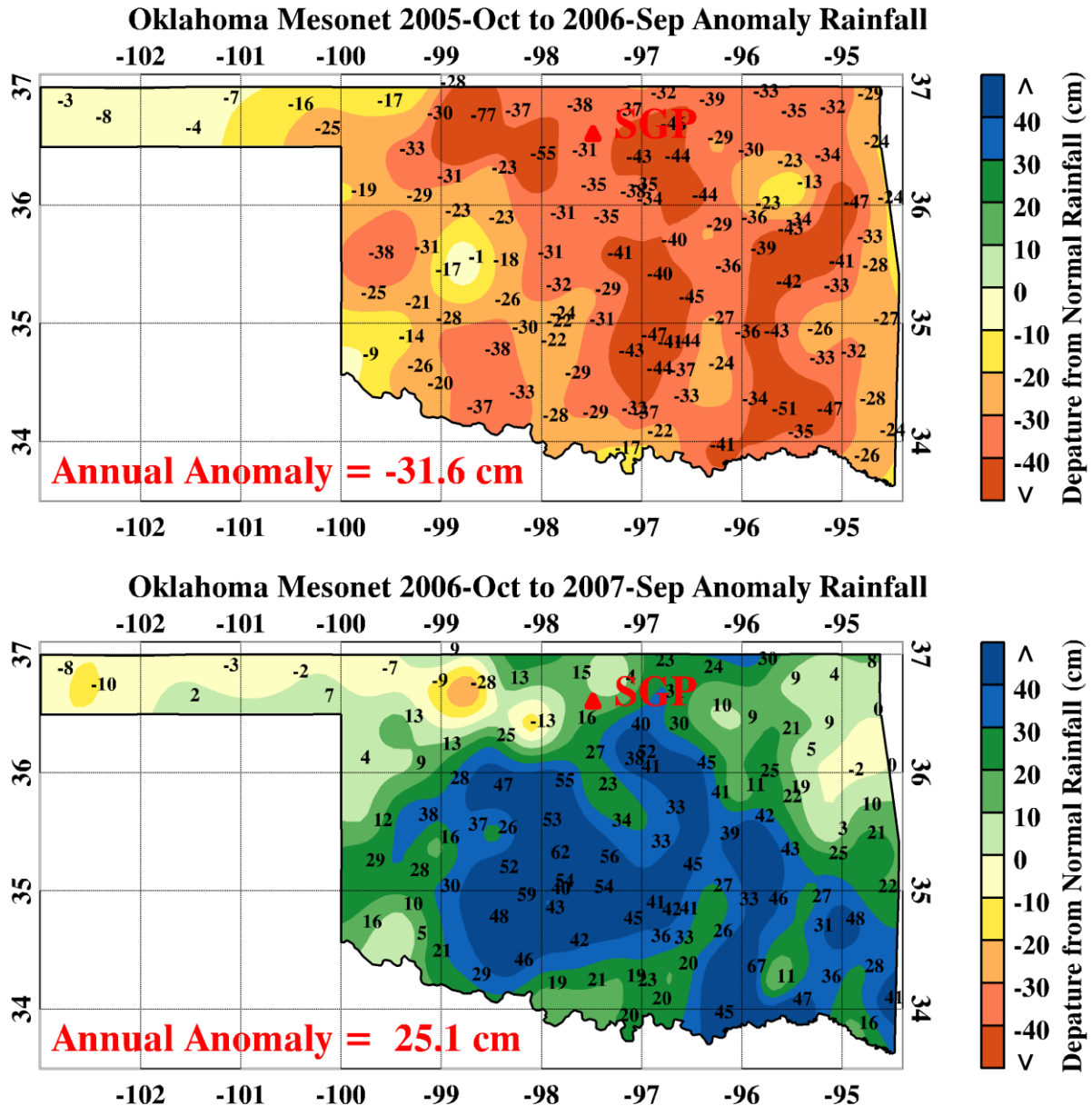
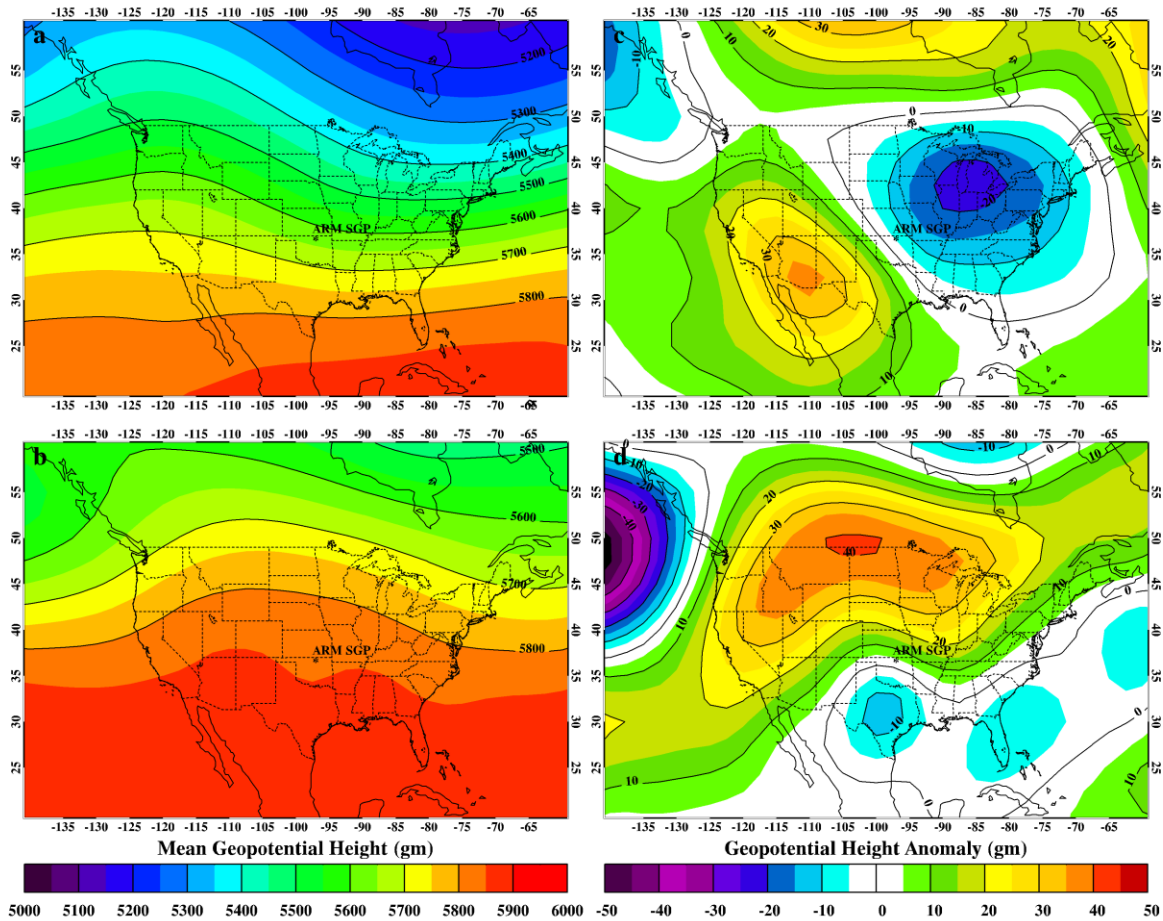


Figure 2. Annual Oklahoma state precipitation anomalies (relative to the 11-yr mean from 1997 to 2007) for HY06 (upper, 10/2005-09/2009) and HY07 (bottom, 10/2006-09/2007).

776  
777  
778  
779  
780



781  
782

783 Figure 3. 500-hPa mean Geopotential Heights (GH) derived from NECP reanalysis during (a) the  
784 extreme dry period (Nov. 2005-Feb. 2006) and (b) the extreme wet period (May-July 2007), and  
785 (c, d) their anomalies (relative to corresponding averages for the period 1979-2007).  
786

787

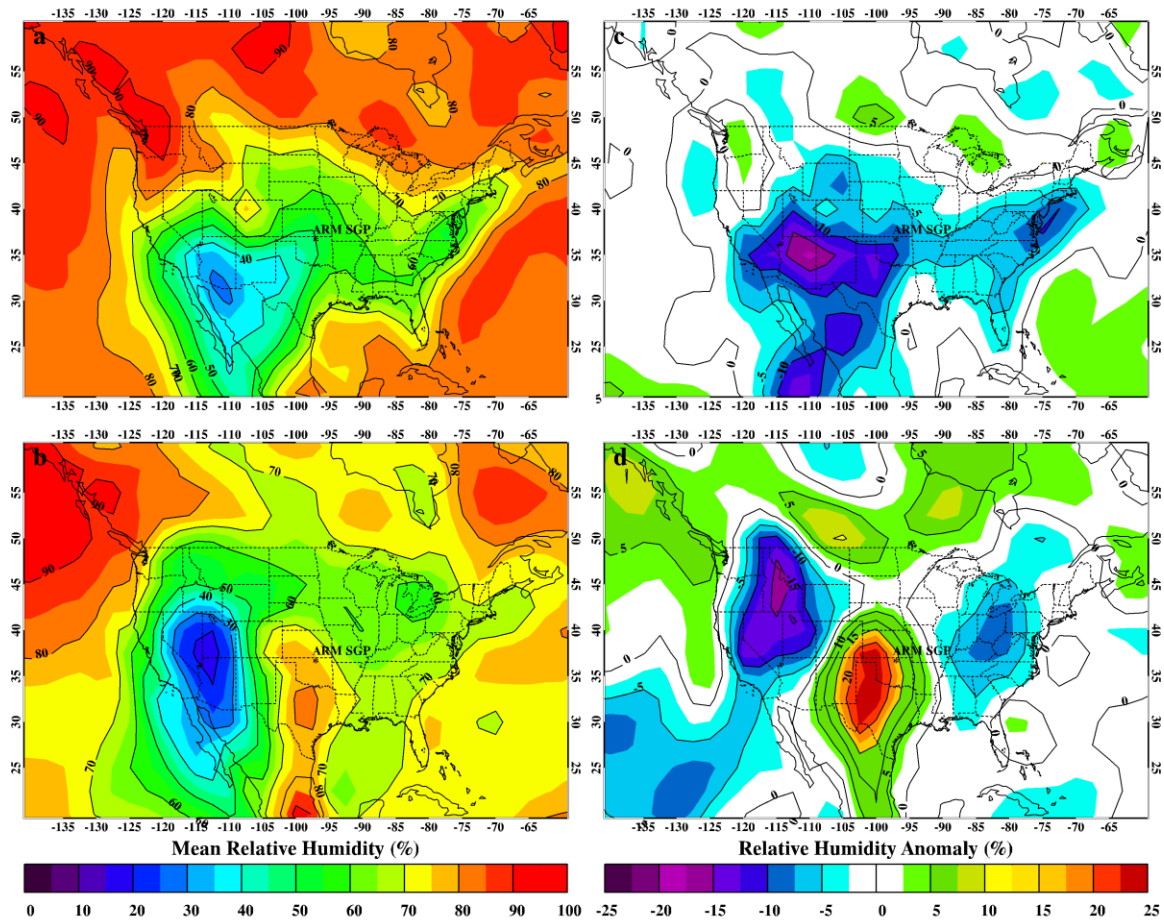


Figure 4. Same as Fig. 3, except for the 925-hPa relative humidity (RH) means (a, b) and anomalies (c, d) during the extreme dry and wet periods.

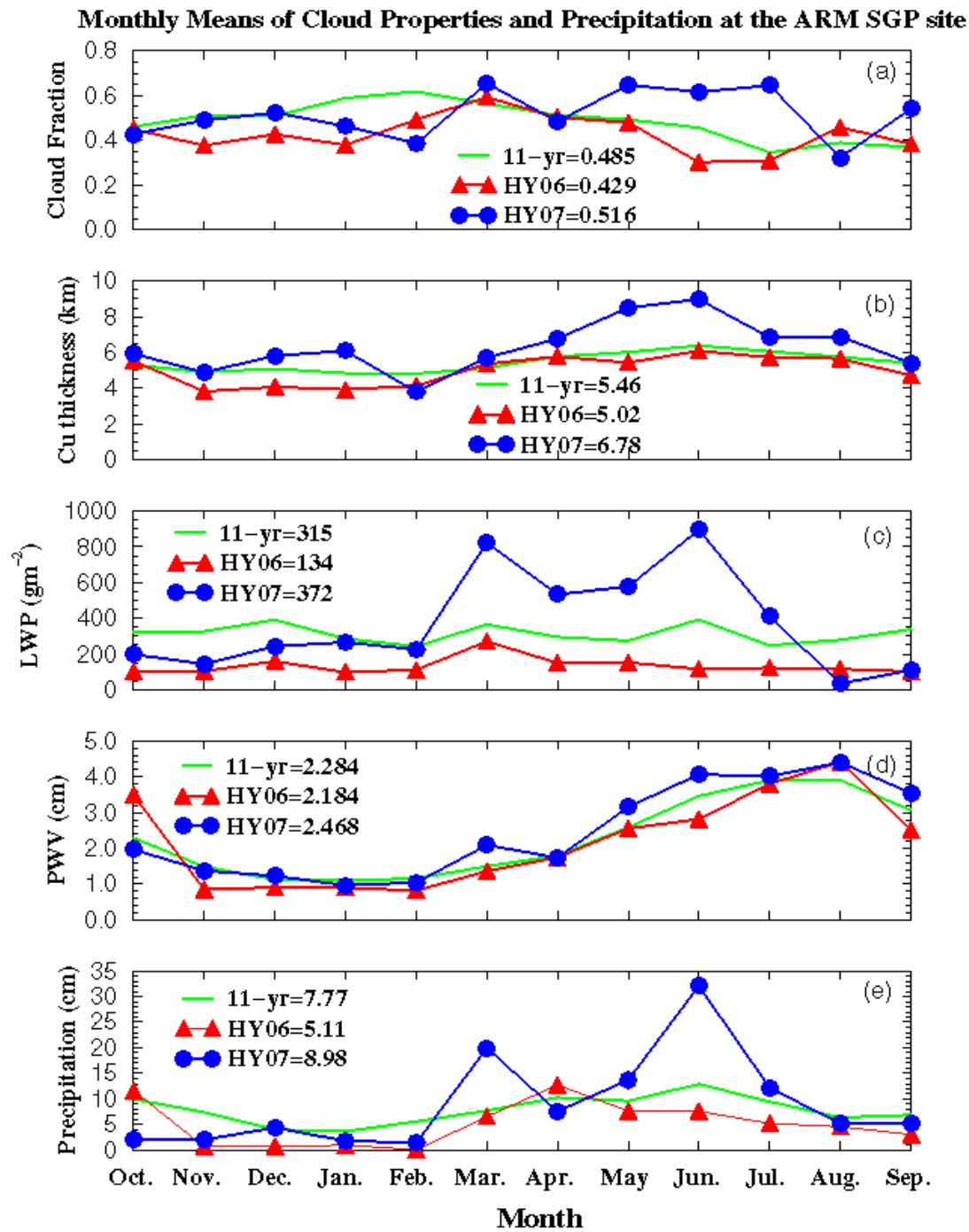


Figure 5. Monthly means of (a) cloud fraction CF and (b) Cumulus (Cu) cloud thickness (contiguous clouds, cloud base<3km and cloud top>6 km) derived from ARM radar-lidar observations, (c) cloud liquid water path (LWP) and (d) atmospheric column precipitable water vapor (PWV) retrieved from microwave radiometer, and (e) surface precipitation measured from rain gauge during HY06, HY07 and 11-yr periods at the ARM SCF.

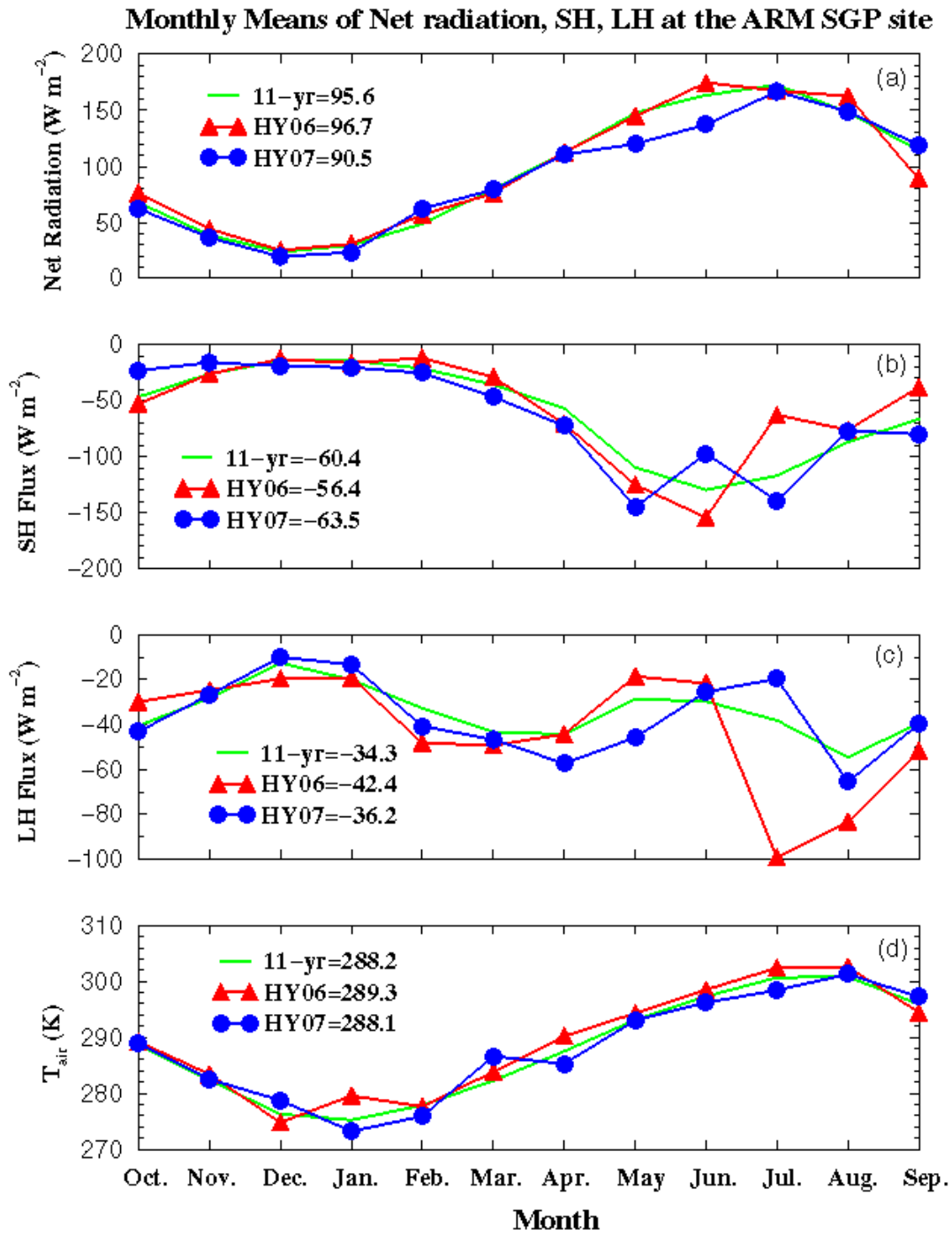


Figure 6. Monthly means of (a) net radiation, (b) sensible heat (SH) flux, (c) latent heat (LH) flux, and (d) surface air temperature ( $T_{\text{air}}$ ) during HY06, HY07, and 11-yr periods measured by the ARM SCF energy balance Bowen ratio system.

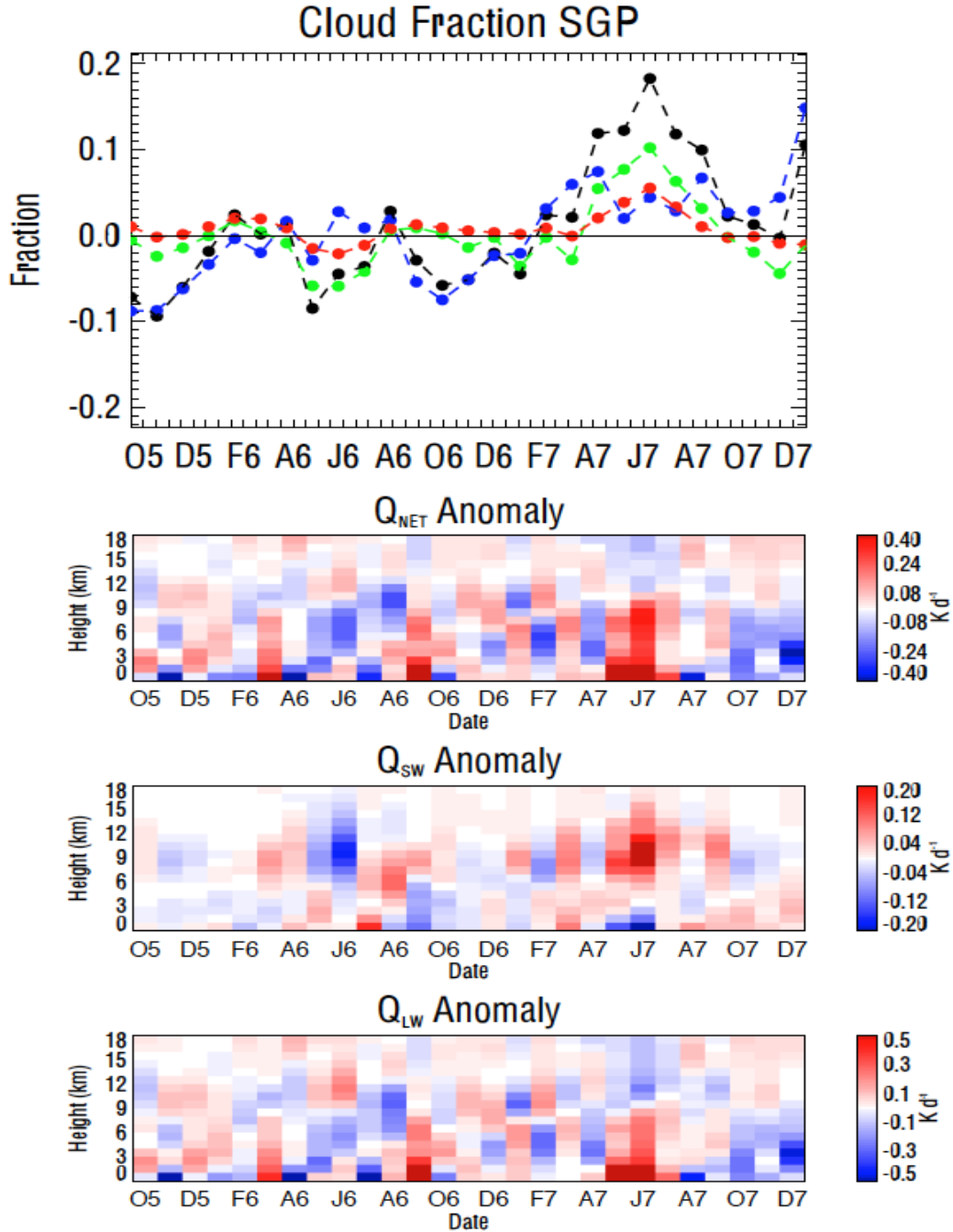
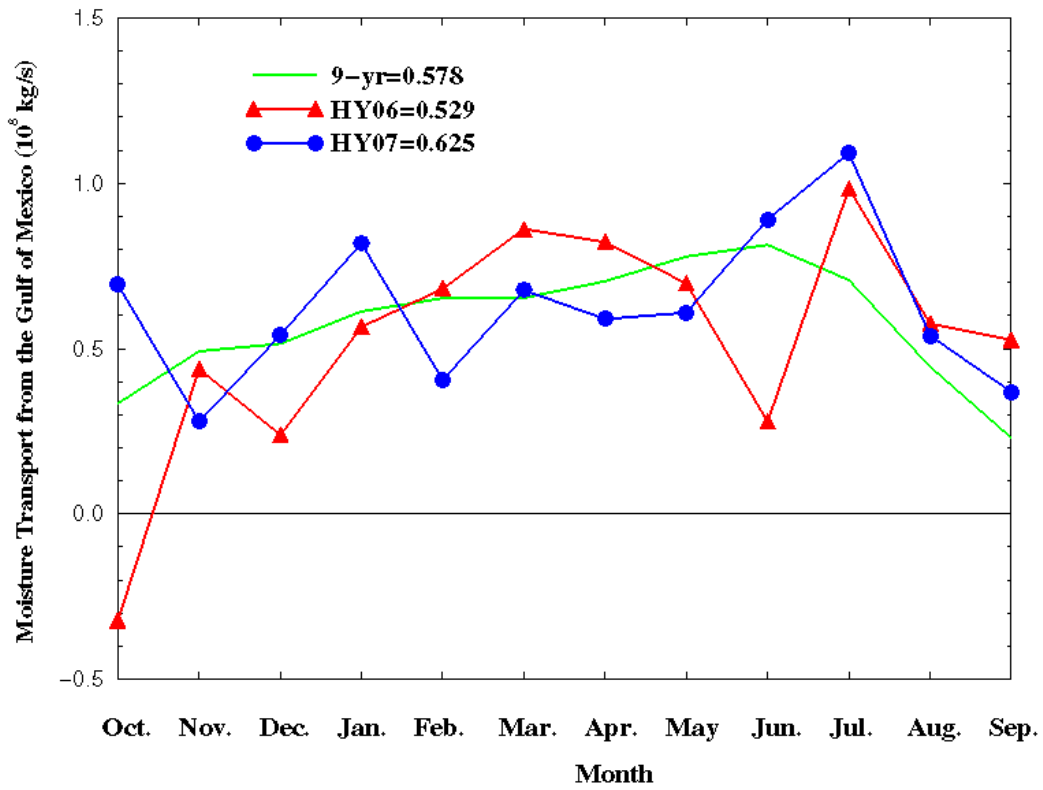


Figure 7. Top: Monthly anomalies (relative to the averages during the period 1998-2007) of raining (red), low (blue), high (green), and total (black) cloud fractions derived from TRMM observations over the broader region of anomalous precipitation (33-38°N and 100-95°W). Corresponding anomalies in NET, SW and LW heating rate profiles are presented in the lower panels. The labels on the abscissa consist of the first letter of the month followed by the last digit of the year and run from October 2005 (O5) through December 2007 (D7).





813

814 Figure 8. Monthly means of meridional component of the vertically integrated moisture  
815 transports from the Gulf of Mexico (positive for northward, 28 °N, 97-90 °W) during HY06,  
816 HY07, and 1999-2007 periods.

817

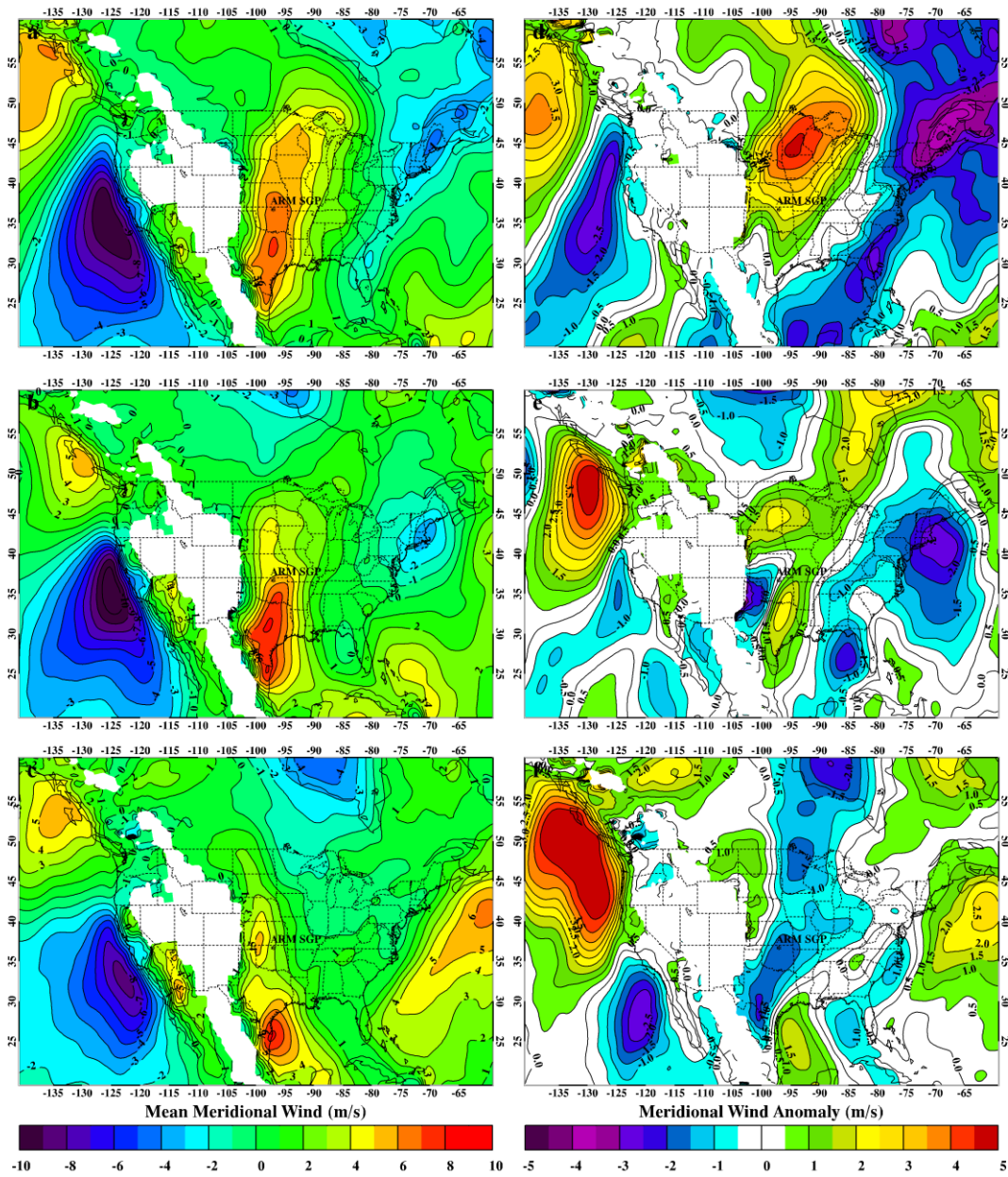


Figure 9. Monthly mean 900-hPa meridional wind (Low Level Jet, LLJ) for (a) May, (b) June, and (c) July. (d)-(f) for monthly anomalies (relative to corresponding averages for 1979-2007).

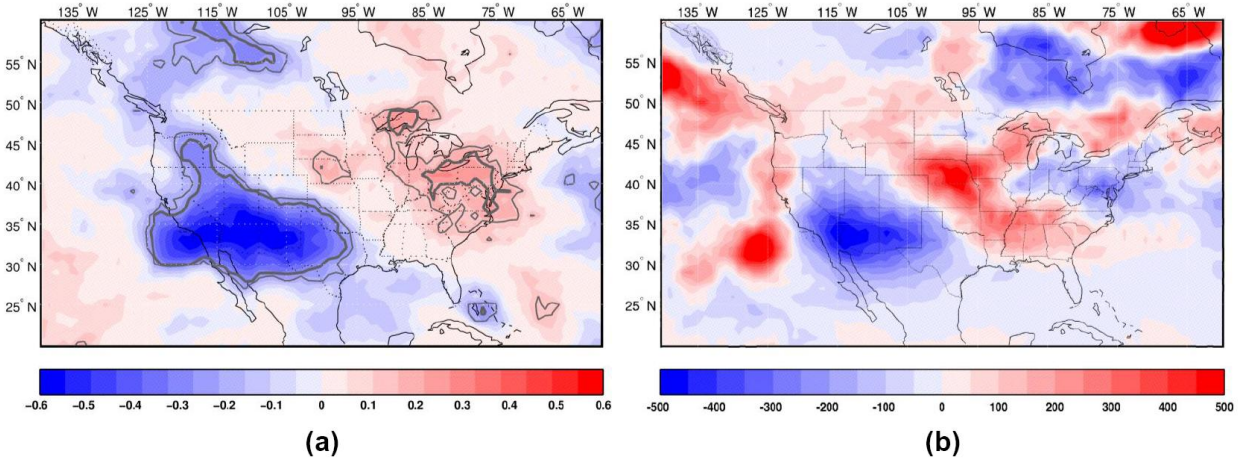


Figure 10. (a) Correlation between the monthly cyclonic activity over the continental U.S. and the precipitation (from the MERRA precipitation) over a grid box of 30-40°N and 105-95°W during the period Nov-Feb., 1979/80-2008/09 (sign of the precipitation is reversed to reflect the drought condition). (b) Anomalies of the cyclonic activity during the extreme dry period (Nov. 2005- Feb. 2006) relative to the 1979/80-2008/09 climatology (color shadings in m per day). Thick (thin) contours in (a) correspond to the 99% (95%) level of statistical significance.

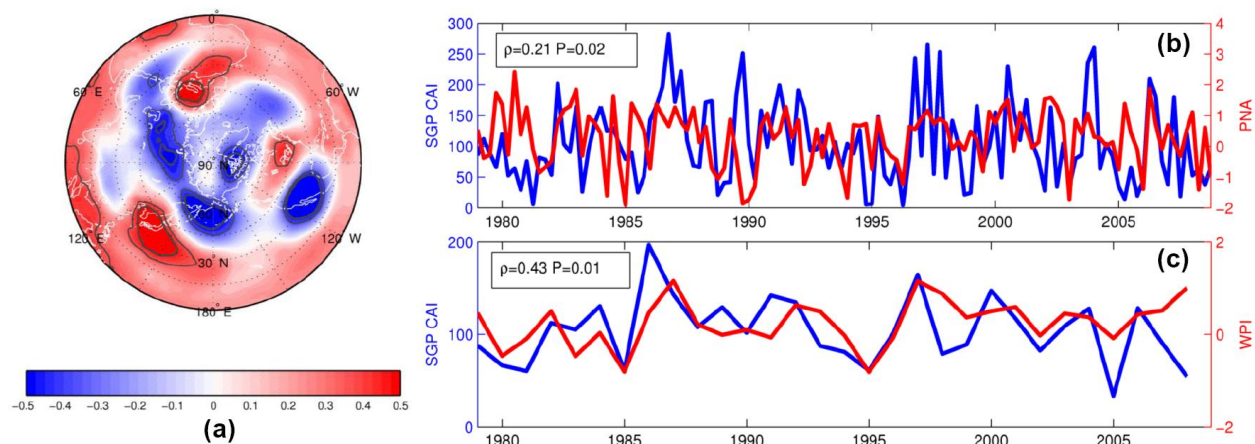


Figure 11. (a) Correlation between the Nov-Feb averaged 500-hPa GH and the cyclonic activity index (CAI), (b) Monthly CAI (blue line) and the corresponding NOAA PNA index (red line) during Nov-Feb, 1979/80-2008/09, (c) Nov-Feb averaged CAI and the corresponding NOAA WP index during Nov-Feb, 1979/80-2008/09. Thick (thin) contours in (a) correspond to the 99% (95%) level of statistical significance. Source of the PNA and WP index: <http://www.cpc.noaa.gov/data/teledoc/telecontents>.

Table 1: Seasonal statistics of precipitation and their severities during 2006-2007 from Oklahoma Climatological Survey (<http://climate.mesonet.org/>)

Seasons	Percentage of normal precipitation	Severities in Oklahoma historical record
<b>HY2006 (10/05 to 09/06)</b>	<b>61%</b>	<b>2<sup>nd</sup> driest</b>
<b>HY2007 (10/06 to 09/07)</b>	<b>121%</b>	<b>7<sup>th</sup> wettest for OK state, 1<sup>st</sup> wettest for central OK</b>
2005 SON	44%	13 <sup>th</sup> driest
2005-2006 DJF	27%	1 <sup>st</sup> driest
2006 MAM	80%	23 <sup>rd</sup> driest
2006 JJA	75%	21 <sup>st</sup> driest
2006 SON	73%	32 <sup>nd</sup> driest
2006-2007 DJF	123%	19 <sup>th</sup> wettest
2007 MAM	117%	13 <sup>th</sup> wettest
2007 JJA	168%	2 <sup>nd</sup> wettest,
2007 SON	63%	21 <sup>st</sup> driest

Note: Normal precipitation=average precipitation (92.84 cm) for the period 1921-2008.

Table 2. The DOE ARM SCF observations and other data sets used in this study

Parameter	Instruments/Methods	Used in the paper	References
Drought Index	Palmer Drought Severity Index (PDSI)	Section 3.1. Fig. 1	Alley (1984)
Surface precipitation	ARM SCF tipping bucket rain gauge	Section 3.1. Fig. 1	ARM website <a href="http://www.arm.gov">www.arm.gov</a>
Surface Precipitation	GPCP Version 2	Section 3.1. Fig. 1	Adler et al. (2003)
Surface precipitation	Oklahoma Mesonet	Section 3.1. Figs. 1 and 2	Brock et al. (1995)
CF, moisture flux, and surface precipitation	TRMM TMI/VIRS and 2A12 rainfall product	Sections 3.1, 3.3, and 3.4. Figs. 1, 7, and 8.	Kummerow et al. (2000)
500-hPa GH, 925-hPa RH, and low level jet	NCEP reanalysis	Section 3.2. Figs. 3,4, and 9	Kalnay et al. (1996)
Cloud fraction (CF)	Radar-lidar observations	Section 3.3. Fig. 5	Dong et al. (2006)
Cumulus cloud thickness	Radar-lidar observations	Section 3.3. Fig. 5	Clothiaux et al. (2000)
Cloud LWP and atmospheric PWV	Microwave radiometer	Section 3.3. Fig. 5	Dong et al. (2000); Liljegren et al. 2001
Latent Heat, Sensible heat, and NET Radiation	Energy Balance Bowen Ratio Station	Section 3.3. Fig. 6	ARM website <a href="http://www.arm.gov">www.arm.gov</a>
Surface air temperature	ARM SCF surface Meteo. Instrumentation	Section 3.3. Figs. 6	ARM website <a href="http://www.arm.gov">www.arm.gov</a>
CAI, PNA, and WP Index	NASA MERRA reanalysis	Section 3.4. Figs. 10 and 11	Wallace and Gutzler (1981)

879 Table 3a. Correlations of monthly means (10/2005-09/2007)

Parameter	CF	Cu $\Delta Z$	LWP	PWV	Precip	Net_Rad	SH	LH	T <sub>air</sub>
CF, phase	1	<b>0.464</b>	<b>0.715</b>	0.085	<b>0.600</b>	0.043	-0.218	0.209	-0.041
1-m early		<b>0.539</b>	<b>0.362</b>	0.117	<b>0.441</b>	0.292	-0.347	0.282	0.053
1-m late		0.220	<b>0.417</b>	-0.148	0.198	-0.077	0.215	-0.270	-0.224
Cu $\Delta Z$		1	<b>0.639</b>	<b>0.622</b>	<b>0.740</b>	<b>0.665</b>	<b>-0.658</b>	-0.091	<b>0.509</b>
			0.272	<b>0.696</b>	<b>0.463</b>	<b>0.627</b>	<b>-0.620</b>	-0.001	<b>0.563</b>
			<b>0.652</b>	0.266	<b>0.495</b>	<b>0.464</b>	<b>-0.554</b>	-0.177	0.298
LWP			1	0.139	<b>0.807</b>	0.223	-0.273	0.083	0.018
				0.340	<b>0.507</b>	<b>0.444</b>	<b>-0.499</b>	0.043	0.199
				-0.135	0.273	-0.032	-0.098	-0.071	-0.228
PWV				1	<b>0.490</b>	<b>0.844</b>	<b>-0.681</b>	<b>-0.435</b>	<b>0.916</b>
					0.104	<b>0.533</b>	<b>-0.395</b>	-0.288	<b>0.752</b>
					<b>0.503</b>	<b>0.924</b>	<b>-0.834</b>	<b>-0.391</b>	<b>0.769</b>
Precip					1	<b>0.520</b>	<b>-0.513</b>	0.036	<b>0.388</b>
						<b>0.597</b>	<b>-0.636</b>	0.041	<b>0.470</b>
						0.301	<b>-0.418</b>	-0.174	0.062
Net_Rad						1	<b>-0.851</b>	<b>-0.442</b>	<b>0.893</b>
							<b>-0.664</b>	<b>-0.438</b>	<b>0.953</b>
							<b>-0.838</b>	-0.258	<b>0.620</b>
SH							1	0.039	<b>-0.723</b>
								0.344	<b>-0.829</b>
								0.171	<b>-0.443</b>
LH								1	<b>-0.503</b>
									<b>-0.456</b>
									<b>-0.381</b>
T <sub>air</sub>									1

880  
881 Note: In-phase means the properties are in the same month, 1-month earlier means that CF in January and other  
882 parameters are in February, and 1-month late is reverse. These correlations are in 95% (**bold**) and 99% confidence  
883 levels (**bold and italic**).  
884  
885  
886  
887  
888  
889  
890  
891  
892  
893  
894  
895  
896  
897  
898  
899  
900  
901  
902  
903

904 Table 3b. Correlations of monthly anomalies (10/2005-09/2007)

Parameter	CF	Cu ΔZ	LWP	PWV	Precip	Net_Rad	SH	LH	T <sub>air</sub>
CF, phase	1	<b>0.568</b>	<b>0.495</b>	<b>0.529</b>	<b>0.575</b>	<b>-0.465</b>	-0.117	0.092	-0.066
1-m early		<b>0.482</b>	0.058	0.174	0.167	-0.347	-0.019	0.305	<b>-0.378</b>
1-m late		<b>0.508</b>	<b>0.498</b>	0.262	<b>0.381</b>	-0.285	0.248	<b>-0.376</b>	-0.173
Cu_ΔZ		1	<b>0.683</b>	<b>0.544</b>	<b>0.650</b>	<b>-0.615</b>	-0.117	0.091	-0.202
			<b>0.432</b>	<b>0.408</b>	<b>0.423</b>	-0.322	-0.142	0.288	<b>-0.529</b>
			<b>0.647</b>	0.163	0.307	<b>-0.458</b>	-0.230	-0.110	-0.247
LWP			1	<b>0.384</b>	<b>0.782</b>	<b>-0.460</b>	-0.139	0.038	-0.152
				<b>0.438</b>	<b>0.508</b>	-0.316	-0.319	0.192	<b>-0.465</b>
				0.214	<b>0.386</b>	-0.246	-0.292	-0.122	-0.206
PWV				1	<b>0.637</b>	-0.118	-0.141	0.034	0.135
					0.204	-0.121	-0.228	<b>0.385</b>	-0.279
					0.109	-0.187	-0.038	-0.302	<b>-0.375</b>
Precip					1	<b>-0.424</b>	-0.061	0.190	0.106
						-0.118	-0.310	0.351	<b>-0.471</b>
						-0.208	-0.306	-0.195	-0.279
Net_Rad						1	-0.212	0.003	0.257
							0.016	<b>-0.427</b>	0.358
							0.229	0.169	0.182
SH							1	<b>-0.565</b>	-0.023
								0.108	0.063
								-0.174	0.077
LH								1	-0.092
									-0.123
									-0.132
T <sub>air</sub>									1

905  
906